



# Crystal Structure of the Monomeric Extracellular Domain of $\alpha 9$ Nicotinic Receptor Subunit in Complex With $\alpha$ -Conotoxin RglA: Molecular Dynamics Insights Into RglA Binding to $\alpha 9\alpha 10$ Nicotinic Receptors

## OPEN ACCESS

Marios Zouridakis<sup>1\*</sup>, Athanasios Papakyriakou<sup>2</sup>, Igor A. Ivanov<sup>3</sup>, Igor E. Kasheverov<sup>3,4</sup>, Victor Tsetlin<sup>5</sup>, Socrates Tzartos<sup>1,6</sup> and Petros Giastas<sup>1,2\*</sup>

### Edited by:

Mounir Tarek,  
Centre National de la Recherche  
Scientifique (CNRS), France

### Reviewed by:

Vishwanath Jogini,  
D. E. Shaw Research, United States  
Chris Ulens,  
KU Leuven, Belgium  
Marco Cecchini,  
Université de Strasbourg, France

### \*Correspondence:

Petros Giastas  
petrosgiastas@gmail.com  
Marios Zouridakis  
marzouri@gmail.com

### Specialty section:

This article was submitted to  
Pharmacology of Ion Channels  
and Channelopathies,  
a section of the journal  
Frontiers in Pharmacology

**Received:** 15 November 2018

**Accepted:** 15 April 2019

**Published:** 01 May 2019

### Citation:

Zouridakis M, Papakyriakou A,  
Ivanov IA, Kasheverov IE, Tsetlin V,  
Tzartos S and Giastas P (2019)  
Crystal Structure of the Monomeric  
Extracellular Domain of  $\alpha 9$  Nicotinic  
Receptor Subunit in Complex With  
 $\alpha$ -Conotoxin RglA: Molecular  
Dynamics Insights Into RglA Binding  
to  $\alpha 9\alpha 10$  Nicotinic Receptors.  
*Front. Pharmacol.* 10:474.  
doi: 10.3389/fphar.2019.00474

<sup>1</sup> Department of Neurobiology, Hellenic Pasteur Institute, Athens, Greece, <sup>2</sup> Institute of Biosciences and Applications, NCSR “Demokritos”, Athens, Greece, <sup>3</sup> Shemyakin-Ovchinnikov Institute of Bioorganic Chemistry, Russian Academy of Sciences, Moscow, Russia, <sup>4</sup> Institute of Molecular Medicine, Sechenov First Moscow State Medical University, Moscow, Russia, <sup>5</sup> PhysBio of MEPhI, Moscow, Russia, <sup>6</sup> Department of Pharmacy, University of Patras, Patras, Greece

The  $\alpha 9$  subunit of nicotinic acetylcholine receptors (nAChRs) exists mainly in heteropentameric assemblies with  $\alpha 10$ . Accumulating data indicate the presence of three different binding sites in  $\alpha 9\alpha 10$  nAChRs: the  $\alpha 9(+)/\alpha 9(-)$ , the  $\alpha 9(+)/\alpha 10(-)$ , and the  $\alpha 10(+)/\alpha 9(-)$ . The major role of the principal (+) side of the extracellular domain (ECD) of  $\alpha 9$  subunit in binding of the antagonists methyllycaconitine and  $\alpha$ -bungarotoxin was shown previously by the crystal structures of the monomeric  $\alpha 9$ -ECD with these molecules. Here we present the 2.26-Å resolution crystal structure of  $\alpha 9$ -ECD in complex with  $\alpha$ -conotoxin ( $\alpha$ -Ctx) RglA, a potential drug for chronic pain, the first structure reported for a complex between an nAChR domain and an  $\alpha$ -Ctx. Superposition of this structure with those of other  $\alpha$ -Ctxs bound to the homologous pentameric acetylcholine binding proteins revealed significant similarities in the orientation of bound conotoxins, despite the monomeric state of the  $\alpha 9$ -ECD. In addition, ligand-binding studies calculated a binding affinity of RglA to the  $\alpha 9$ -ECD at the low micromolar range. Given the high identity between  $\alpha 9$  and  $\alpha 10$  ECDs, particularly at their (+) sides, the presented structure was used as template for molecular dynamics simulations of the ECDs of the human  $\alpha 9\alpha 10$  nAChR in pentameric assemblies. Our results support a favorable binding of RglA at  $\alpha 9(+)/\alpha 9(-)$  or  $\alpha 10(+)/\alpha 9(-)$  rather than the  $\alpha 9(+)/\alpha 10(-)$  interface, in accordance with previous mutational and functional data.

**Keywords:** nicotinic acetylcholine receptors,  $\alpha$ -conotoxins, RglA, structure, molecular modeling, molecular dynamics

**Abbreviations:** ACh, acetylcholine; AChBP, acetylcholine-binding protein; ECD, extracellular domain; MD, molecular dynamics; MLA, methyllycaconitine; nAChRs, nicotinic acetylcholine receptors; RMSD, root mean square deviation;  $\alpha$ -Bgtx,  $\alpha$ -bungarotoxin;  $\alpha$ -Ctx,  $\alpha$ -conotoxin; (+) side, principal side; (-) side, complementary side.

## INTRODUCTION

Nicotinic acetylcholine receptors are the prototypic members of the Cys-loop family of pentameric ligand-gated ion channels, including also the 5-HT<sub>3</sub>, GABA<sub>A</sub>, and glycine receptors (Lester et al., 2004; Sine and Engel, 2006; Albuquerque et al., 2009; Nemezc et al., 2016). Muscle and neuronal nAChRs are found at the neuromuscular junction and in central and peripheral neurons, respectively. Neuronal nAChRs regulate neuronal excitability and neurotransmitter release and, in humans, are composed of a combination of eight  $\alpha$  ( $\alpha 2$ – $7$ ,  $\alpha 9$ – $10$ ) and three  $\beta$  ( $\beta 2$ – $4$ ) subunits, forming either homopentamers or heteropentamers (e.g.,  $\alpha 7$ ,  $\alpha 4\beta 2$ ,  $\alpha 7\beta 2$ , and  $\alpha 9\alpha 10$  nAChRs) (Albuquerque et al., 2009; Millar and Gotti, 2009; Engel et al., 2015). These receptors are also found in the immune system and in various peripheral tissues (Wessler and Kirkpatrick, 2008; Beckmann and Lips, 2013). Each neuronal nAChR subtype has distinct pharmacological and electrophysiological properties and distinct localization within the central and peripheral nervous system (Gotti et al., 2006, 2007; Millar and Gotti, 2009; Taly et al., 2009).

Due to their implications in smoking addiction and in various neurological and non-neurological diseases and disorders (e.g., Alzheimer's and Parkinson's diseases, schizophrenia, neuropathic pain, and inflammation), neuronal nAChRs are important drug targets (Taly et al., 2009; Quik et al., 2011; Dineley et al., 2015; Hone and McIntosh, 2018). However, due to the high similarity in the orthosteric ligand-binding site of neuronal nAChRs, the development of drugs targeting specifically a distinct nAChR subtype is a very challenging task, requiring detailed structural information. This site consists of loops A, B, and C of the principal (+) side of the ECD of an  $\alpha$  subunit and of loops D, E, and F of the complementary (–) side of the ECD of the adjacent  $\alpha$  or  $\beta$  subunit (Brejc et al., 2001; Unwin, 2005). Whereas the highly conserved (+) side of the ligand-binding site seems to play an important role in the orientation of the bound ligand (Dellisanti et al., 2007; Zouridakis et al., 2014), it is the less conserved (–) side that determines the selectivity on a specific nAChR subtype (Rucktooa et al., 2009; Bourne et al., 2015; Giastas et al., 2018).

Apart from the early breakthrough cryo-electron microscopy studies of the *Torpedo* muscle-type nAChR (Unwin, 1995, 2005), our understanding of the structure of neuronal nAChR ligand-binding sites was greatly advanced by the X-ray crystal structures of the molluscan AChBPs (Brejc et al., 2001; Celie et al., 2004). AChBPs share up to 24% sequence identity with the ECDs of nAChRs and, most importantly, almost all residues that are conserved in the ligand-binding sites of nAChRs are also found in them. In addition, the X-ray structures of mutated or chimeric AChBPs, carrying single-point mutations or region replacements, respectively, to mimic some nAChR-ECDs, have shed light on the structure of the ligand-binding sites formed between  $\alpha 7$  or  $\alpha 4$  or between  $\alpha 3$  and  $\beta 4$  nAChR subunits (Li et al., 2011; Nemezc and Taylor, 2011; Shahsavari et al., 2015; Abraham et al., 2017). Recent breakthrough X-ray and electron microscopy studies of the almost intact  $\alpha 4\beta 2$  nAChR (Morales-Perez et al., 2016;

Walsh et al., 2018) with nicotine bound, elucidated the 3D structure of  $\alpha 4(+)/\alpha 4(-)$  and  $\alpha 4(+)/\beta 2(-)$  binding sites in high detail. Also, the crystal structure of the  $\alpha 2(+)/\alpha 2(-)$  binding site, present in  $\alpha 2\beta 2$  nAChRs, was solved previously with the agonist epibatidine bound (Kouvatsos et al., 2016), succeeding the crystal structure of the monomeric  $\alpha 9$ -ECD in its free and antagonist [methyllycaconitine (MLA) or  $\alpha$ -bungarotoxin ( $\alpha$ -Bgtx)]-bound forms (Zouridakis et al., 2014).

Subtype-specific inhibitors of nAChRs, apart from valuable tools for dissecting the roles of the various nAChRs, may also be important therapeutic agents. A good example of subtype-specific nAChR antagonists are  $\alpha$ -conotoxins ( $\alpha$ -Ctxs), peptides isolated from the venom of snails belonging to the *Conus* genus (see reviews Nicke et al., 2004; Janes, 2005; Azam and McIntosh, 2009; Rucktooa et al., 2009; Tsetlin et al., 2009).  $\alpha$ -Ctxs range in size from 12 to 19 amino acid residues and contain two disulfide bonds with a Cys1-Cys3 and Cys2-Cys4 connectivity, forming two backbone loops (loop 1 and loop 2, respectively). RgIA, on which the present study is focused, is a 4/3 subclass  $\alpha$ -Ctx (containing four and three residues in loops 1 and 2, respectively), and is highly selective for the  $\alpha 9\alpha 10$  nAChR (Ellison et al., 2006, 2008; Clark et al., 2008). This neuronal nAChR subtype has two stoichiometries, the  $(\alpha 9)_2(\alpha 10)_3$  and  $(\alpha 9)_3(\alpha 10)_2$  (Plazas et al., 2005; Indurthi et al., 2014), and is mainly expressed in the hair cells of the cochlea (Elgoyhen et al., 1994, 2001) and in a variety of immune cells (Lustig et al., 2001; Peng et al., 2004; Hecker et al., 2015). Mutational and functional data suggest that there are three ligand-binding sites in  $\alpha 9\alpha 10$  nAChRs, namely the  $\alpha 9(+)/\alpha 9(-)$ ,  $\alpha 9(+)/\alpha 10(-)$  and the  $\alpha 10(+)/\alpha 9(-)$  (Ellison et al., 2008; Indurthi et al., 2014; Azam et al., 2015; Boffi et al., 2017).

There are many X-ray structures of different AChBPs in complexes with various  $\alpha$ -Ctxs, but here we present the first X-ray crystal structure of an  $\alpha$ -Ctx (RgIA) bound to the nAChR  $\alpha 9$ -ECD, solved at 2.26-Å resolution. As the protein is in a monomeric state, the interactions of RgIA with the (+) side of the  $\alpha 9$ -ECD were revealed and were found to be similar to those between the (+) side of AChBP protomer and, the similar to RgIA,  $\alpha 4/3$ -Ctx ImI (Hansen et al., 2005; Ulens et al., 2006). Moreover, RgIA in its complex with  $\alpha 9$ -ECD superimposed very well with other  $\alpha$ -Ctxs bound to pentameric AChBPs, denoting that the  $\alpha 9(+)$  side in  $\alpha 9\alpha 10$  nAChRs is instrumental for the orientation of the bound RgIA, similarly to what was previously shown for MLA and  $\alpha$ -Bgtx binding to  $\alpha 9$ -ECD (Zouridakis et al., 2014). In addition, based on the crystal structure of  $\alpha 9$ -ECD/RgIA, MD simulations of the complexes of RgIA at  $\alpha 9(+)/\alpha 9(-)$ ,  $\alpha 9(+)/\alpha 10(-)$ , and  $\alpha 10(+)/\alpha 9(-)$  binding sites in human nAChR  $\alpha 9\alpha 10$ -ECDs were performed. These studies indicated that the favorable binding sites for RgIA are the  $\alpha 9(+)/\alpha 9(-)$  and/or  $\alpha 10(+)/\alpha 9(-)$ , rather than the  $\alpha 9(+)/\alpha 10(-)$ , in accordance with previous mutational and functional data. Since the  $\alpha 9\alpha 10$  nAChR is a possible pharmacotherapeutic target for the auditory disease tinnitus and for the chronic neuropathic pain (Elgoyhen et al., 2009; Elgoyhen and Langguth, 2010; Hone and McIntosh, 2018), this study may provide useful information for the design of highly selective improved RgIA analogs for use against such diseases.

## MATERIALS AND METHODS

### Materials

The materials and reagents used for purification and deglycosylation of nAChR  $\alpha 9$ -ECD were Ni<sup>2+</sup>-NTA resin (Qiagen, United States) and EndoH<sub>f</sub> (NEB, United States). All other chemicals used were of analytical grade (SIGMA-ALDRICH, United States). For the solid-phase peptide synthesis of  $\alpha$ -Ctx RgIA, we used: Fmoc-protected amino acids and diisopropylcarbodiimide (Iris Biotech GmbH, Germany), a block-copolymer resin Tentagel HL-NH2 modified with Knorr linker (Tentagel-RAM, Rapp Polymere, Germany), 4-methylpiperidine (Acros Organics, Belgium), hydroxybenzotriazole (Riyin Group, China), trifluoroacetic acid (Solvay Chemicals, Belgium). Other reagents were acquired from local supplier. All reagents and solvents were used without additional purification.

### Protein Expression and Purification

The human nAChR  $\alpha 9$ -ECD was expressed as a C-terminal six-histidine tagged protein in the yeast *Pichia pastoris* system and purified by metal affinity and size exclusion chromatography (SEC); enzymatic deglycosylation was carried out with endoglycosidase EndoH<sub>f</sub>, as also described in Zouridakis et al. (2014).

### Ligand-Binding and Competition Experiments

Ligand-binding experiments to test [<sup>125</sup>I] $\alpha$ -Bgtx binding to the glyco- and deglycosylated  $\alpha 9$ -ECD were described and performed previously (Zouridakis et al., 2014). The K<sub>d</sub> values of [<sup>125</sup>I] $\alpha$ -Bgtx for the glyco- and deglycosylated protein were 30 and 19 nM, respectively (Zouridakis et al., 2014). Competition experiments of [<sup>125</sup>I] $\alpha$ -Bgtx binding to the  $\alpha 9$ -ECD by  $\alpha$ -Ctx RgIA were performed with SEC-purified monomeric glycosylated or deglycosylated histidine-tagged  $\alpha 9$ -ECD bound to Ni<sup>2+</sup>-NTA beads. The beads were washed twice with 10 volumes of phosphate buffer saline (PBS) and then diluted 10 times with PB-BSA buffer [10 mM potassium phosphate buffer, 0.2% bovine serum albumin (BSA), 0.05% NaN<sub>3</sub>, pH 7.4]; 10  $\mu$ l of this dilution were used in each reaction. The protein concentration was 100 nM and the specific activity of [<sup>125</sup>I] $\alpha$ -Bgtx was 30 cpm fmol<sup>-1</sup>. Reaction volume was fixed to 50  $\mu$ l by addition of PB-BSA buffer. Competition experiments were performed with fixed [<sup>125</sup>I] $\alpha$ -Bgtx concentration at 50 nM and variable unlabeled RgIA concentrations (1 nM–200  $\mu$ M). Serial dilutions of the stock buffer of RgIA (initial concentration of 4.8 mM) were done in PB-BSA buffer. Incubation of reaction mixtures was performed overnight at 4°C. The beads were then washed three times in 1 ml of 20 mM Tris and 0.05% Triton X-100, pH 7.5, followed by a final centrifugation at 1000 g, 5 min at 4°C. Finally, the bound radioactivity was measured on a gamma counter. Non-specific binding was measured in samples with the same ingredients but without the  $\alpha 9$ -ECD. All assays were performed in triplicate, and binding data were evaluated with an algorithm of GraphPad Prism 5.0 (GraphPad Software), accounting for ligand depletion.

All numerical data are presented as mean  $\pm$  SEM for at least three independent experiments.

### Synthesis of $\alpha$ -Ctx RgIA Globular Isomer

The globular isomer of  $\alpha$ -Ctx RgIA was synthesized similarly to Ellison et al. (2008) by the solid-phase method, using Fmoc-protected amino acids with the Trt- and AcM- protection of cysteines for the first (1–3) and second (2–4) disulfide bonds, respectively, and DIC/HOBt as a coupling reagent. Linear peptide was totally deprotected and cleaved from the polymer with TFA/DTT/H<sub>2</sub>O 93:4:3 cocktail. A crude peptide was isolated by ether precipitation and subsequent purification was performed on YMC Triart C18 10 u 150 mm  $\times$  30 mm column, using Gilson 333/334 binary gradient HPLC system with spectrophotometric detection at 210-nm wavelength. The purified linear RgIA was subjected to a closure of the first disulfide bond by atmospheric oxygen at high pH. Briefly, linear peptide was dissolved in aqueous 50 mM ammonium bicarbonate to a final concentration of 0.5 g/L, stirred on air for 72 h and lyophilized. Purification of monocyclic intermediate was performed under the same conditions as linear ones. Deprotection of AcM-protected cysteines and oxidation were performed by treatment with iodine solution in glacial acetic acid. Excess of iodine was quenched by aqueous citric acid. The reaction mixture was freeze-dried, and the final product was purified on a C8 reverse-phase column. Its purity was confirmed by UPLC/MS analysis.

### Crystallization and Data Collection

Crystals of the deglycosylated  $\alpha 9$ -ECD in complex with  $\alpha$ -Ctx RgIA were grown by the sitting-drop vapor-diffusion method in 100 mM HEPES, pH 7.5, 20% PEG 10000 at a protein concentration of 3.5 mg ml<sup>-1</sup> and a molar ratio of protein to RgIA equal to 1:3. Cryoprotection of the crystals was achieved by immersion in a solution containing the precipitant and 20% ethylene glycol for  $\sim$ 10 s. Subsequently, the crystals were vitrified in liquid N<sub>2</sub>. Data were collected at 100 K at a wavelength of 1.0 Å on beamline I04 of the Diamond Light Source, Didcot, United Kingdom. The reflections were integrated with XDS (Kabsch, 2010), the space group was determined with POINTLESS (Evans, 2011), and the data merging was carried out with SCALA (Evans, 2006) of the CCP4 (Winn et al., 2011) suite.

### Structure Determination and Refinement

The structure of the  $\alpha 9$ -ECD/RgIA complex was solved by molecular replacement with PHASER (McCoy et al., 2007), using as a search model the apo structure of  $\alpha 9$ -ECD (PDB ID: 4D01) (Zouridakis et al., 2014). The electron density maps clearly showed the presence of a large and continuous electron density in the binding site region, attributed to  $\alpha$ -Ctx RgIA. The structure was refined with PHENIX (Afonine et al., 2012) with restrained refinement and TLS refinement implemented in the final stages. Model building and real-space refinement were performed in COOT (Emsley et al., 2010). The high-resolution limit was determined with the CC1/2 and mean (I/ $\sigma$ I) criteria (Karplus and Diederichs, 2012), using as cutoff the values of 60% and 1.5, respectively. Almost 99% of the residues of  $\alpha 9$  ECD were in Ramachandran favored or allowed regions, and 1% were outliers,

whereas the overall geometry inspection showed no outliers in rotameric and omega angle analyses. The electron density for the region 102–104 of  $\alpha$ 9-ECD could not be determined and therefore the corresponding residues were not built in the model. The atomic coordinates and structure factors of the  $\alpha$ 9-ECD/RgIA complex were deposited in the Protein Data Bank, under the accession code 6HY7. The PyMOL program<sup>1</sup> was used for structure visualization and for generation of the figures.

## Computational Methods

The homology model of human nAChR  $\alpha$ 10-ECD was based on the X-ray crystal structure of human  $\alpha$ 9-ECD complex with the  $\alpha$ -Ctx RgIA presented here (PDB ID: 6HY7). All non-protein atoms were removed from the template structure. Sequence alignment between human  $\alpha$ 9 and  $\alpha$ 10 ECDs (**Figure 2D**) was performed using Clustal Omega and the UNIPROT accession codes Q9UGM1 and Q9GZZ6 for  $\alpha$ 9 and  $\alpha$ 10, respectively (67% sequence identity for 212 residues). From a total of 30 homology models of human  $\alpha$ 10-ECD that were generated using Modeller v9.10 (Fiser and Sali, 2003), we selected the lowest DOPE score model, which was used without any further optimization. The models of pentameric ( $\alpha$ 9)<sub>2</sub>( $\alpha$ 10)<sub>3</sub> and ( $\alpha$ 9)<sub>3</sub>( $\alpha$ 10)<sub>2</sub> ECDs were prepared by superimposing the two human monomers (either free or RgIA-bound) on the crystallographic structure of the *Aplysia californica* AChBP in complex with  $\alpha$ -Ctx ImI (PDB ID: 2C9T) (Ulens et al., 2006), using the MULTISEQ plugin of VMD v1.9.4 (Humphrey et al., 1996). RgIA was placed at only one binding site in the modeled pentamers, formed between either  $\alpha$ 9(+)/ $\alpha$ 9(-), or  $\alpha$ 9(+)/ $\alpha$ 10(-), or between  $\alpha$ 10(+)/ $\alpha$ 9(-) interfaces.

## Molecular Dynamics (MD) Simulations

Molecular dynamics simulations were performed using the GPU-accelerated version of PMEMD in AMBER v16 (Case et al., 2005; Salomon-Ferrer et al., 2013) and the ff14SB force field parameters (Maier et al., 2015). The systems were solvated in truncated octahedron boxes of TIP3P waters with a minimum extension of 12 Å from the solute and the total charge was neutralized with the addition of sodium ions. All simulations were performed with a 4-fs time step by applying the hydrogen mass repartitioning method (Hopkins et al., 2015). The Particle Mesh Ewald method was used for long-range electrostatic interactions with a real space cutoff of 9 Å. Temperature was regulated using a Langevin thermostat with a collision frequency of 1.0 ps<sup>-1</sup> and the pressure was regulated at 1.0 bar using the Berendsen weak-coupling algorithm with a relaxation time of 1.0 ps. First, each system was energy minimized without restraints for 2000 steps to remove steric clashes. Then, the temperature was increased to 200 K within 100 ps under constant volume (NVT ensemble), using harmonic positional restraints of 100 kcal/mol Å<sup>2</sup> on all protein atoms. Within the next 200 ps, temperature was increased to 300 K under constant pressure (NPT ensemble), while reducing the restraints to 50 kcal/mol Å<sup>2</sup>. Pressure equilibration was performed for a total of 2 ns at 300 K in the NPT with restraints applied only on the (+) side and

RgIA C $\alpha$  atoms. These restraints were gradually decreased from 25 to 1.0 kcal/mol Å<sup>2</sup> within the first 1 ns of equilibration and were retained during the remaining equilibration. In subsequent unrestraint production simulations of 0.5  $\mu$ s at 300 K in the canonical ensemble (NVT) we observed that RgIA sampled a large conformational space rendering analysis of residue-specific interactions at either (+) or (-) sides very difficult. Therefore, we retained weak restraints of 1.0 kcal/mol Å<sup>2</sup> only on the 211 C $\alpha$  atoms of the  $\alpha$ 9 or  $\alpha$ 10 ECD comprising each time the (+) side of the binding site and on the 13 C $\alpha$  atoms of RgIA for 0.2  $\mu$ s of the production runs. These restraints were then reduced to 0.1 kcal/mol Å<sup>2</sup> for additional 0.2  $\mu$ s, while the side chains of all residues were kept unrestrained during the whole simulation time. In contrast, the ECD participating at the (-) side of the binding site and the other three ECDs in each pentameric system were unrestrained, allowing for the sampling of potential interactions of RgIA with the (-) side of the  $\alpha$ 9 or  $\alpha$ 10 ECD. Trajectory snapshots were collected every 10 ps and were processed using the CPPTRAJ module of AMBER. The non-bonded interaction energy terms (electrostatic and van der Waals) between RgIA and the nAChR ECDs were calculated within the LIE methodology implemented in CPPTRAJ with the default 12-Å cutoff. Clustering of the trajectory snapshots was performed using a hierarchical agglomerative approach with a minimum distance between clusters of 2.0 Å, after mass-weighted, root-mean-square deviation fitting of the Ca atoms at the two binding subunits of RgIA. Calculations were performed on Linux workstations equipped with NVIDIA GTX 1080 GPUs.

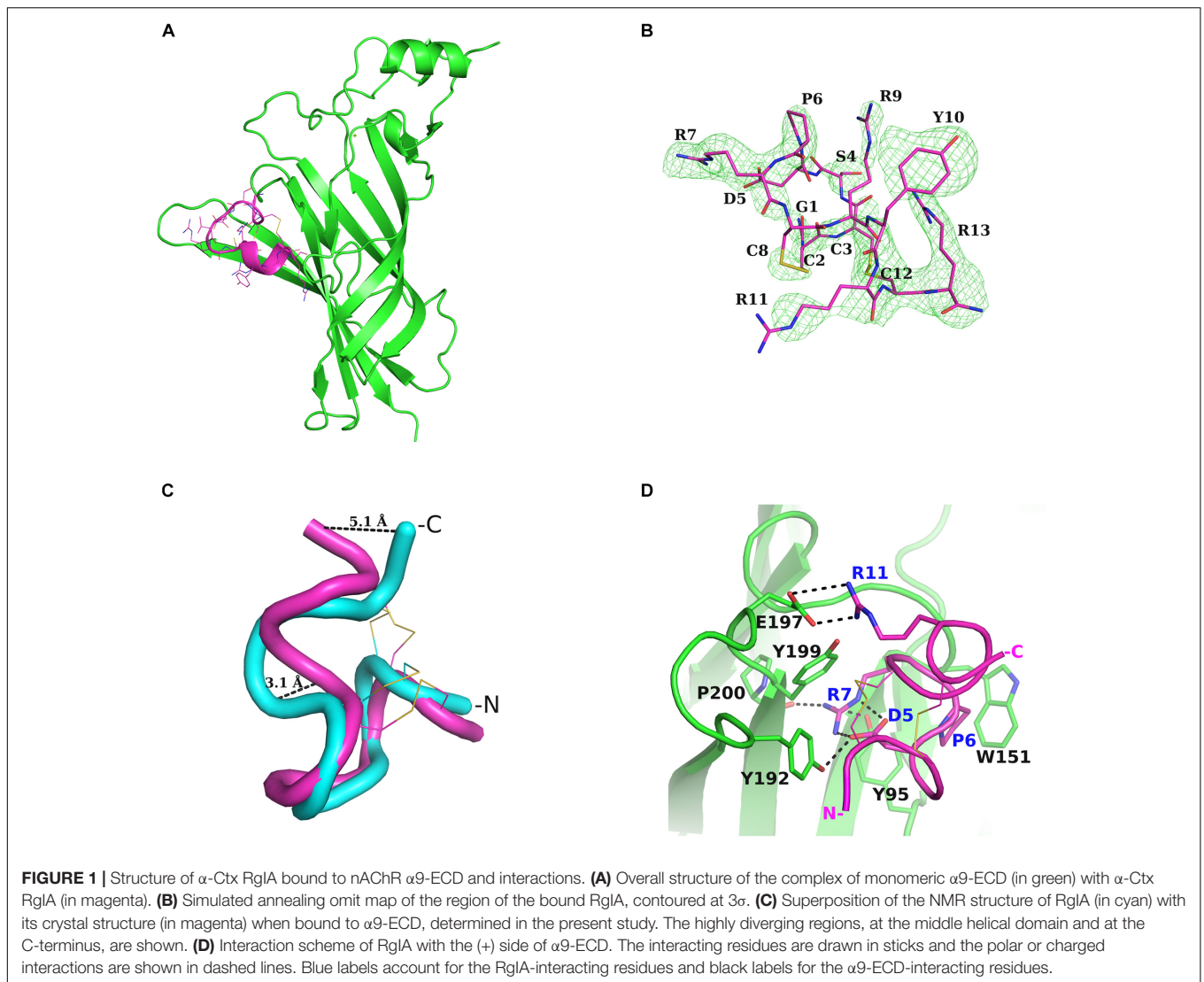
## RESULTS

### Overall Structure of the $\alpha$ 9-ECD/RgIA Complex

The crystal structure of the complex of the deglycosylated human nAChR  $\alpha$ 9-ECD in complex with the C-terminally amidated  $\alpha$ -Ctx RgIA was solved at 2.26-Å resolution (**Figures 1A,B**, **Supplementary Figure S1** and **Supplementary Table S1**). Whereas the structure of the  $\alpha$ 9-ECD in this complex was very similar to the previously determined structure of the apo  $\alpha$ 9-ECD (Zouridakis et al., 2014), presenting a RMSD value of 0.497 Å for their paired C $\alpha$  atoms, the crystal structure of RgIA bound to  $\alpha$ 9-ECD presented an RMSD value for Ca atoms of 1.905 Å compared to its NMR structure in solution (PDB ID: 2JUT) (Ellison et al., 2008). This difference is mainly attributed to the C-terminal Arg13, which upon superposition of the two RgIA structures shows >5 Å distance between their C $\alpha$  atoms, revealing the intrinsic flexibility of this residue (**Figure 1C**). Another notable difference is the  $\alpha$ -helical domain in the middle of the crystallized RgIA molecule, which is missing in the NMR structure of RgIA (**Figure 1C**). In addition, in the crystal structure of RgIA, an intramolecular salt bridge between Asp5 and Arg7 was observed (**Figure 1D**), also missing from its NMR structure.

To investigate whether these observed conformational changes of RgIA upon binding to  $\alpha$ 9-ECD have been reported in other cases, we sought for examples involving  $\alpha$ -Ctxs. When

<sup>1</sup><http://www.pymol.org/>



comparing the NMR structures of PnIA (PDB ID: 1PEN) (Hu et al., 1996), GIC (PDB ID: 1UL2) (Chi et al., 2004), BuIA (PDB ID: 2I28) (Chi et al., 2006) and LvIA (PDB ID: 2MDQ) (Luo et al., 2014) to their crystal complexes with AChBP (PDB IDs: 2BR8 for PnIA; 5CO5 for GIC; 4EZ1 for BuIA; 5XGL for LvIA) (Celie et al., 2005; Lin et al., 2016; Xu et al., 2017), no differences were noticed regarding their backbone conformations. However, in the case of ImI, which is the most similar  $\alpha$ -Ctx to RgIA (**Figure 2B**), two clusters of NMR structures are available; one lacking the  $\alpha$ -helical domain in the middle of the toxin (PDB ID: 1CNL) (Gehrmann et al., 1999), similarly to the sole NMR structure of RgIA (PDB ID: 2JUT) (Ellison et al., 2008), and another where the helical domain is present (PDB ID: 1IMI) (Maslennikov et al., 1999) (**Supplementary Figure S2**), as in its crystal complex with AChBP (PDB ID: 2C9T) (Ulens et al., 2006). Thus, it is not clear whether the observed backbone conformational differences between the crystallized RgIA bound to  $\alpha 9$ -ECD and its NMR structure are induced by its interactions with  $\alpha 9$ -ECD or could

be due to varying in-solution NMR conformational states (as in the case of ImI). Instead, the salt bridge between Asp5 and Arg7 of RgIA is most probably induced by its binding to  $\alpha 9$ -ECD, since this is also apparent in the crystal complex of ImI with AChBP, while lacking from its varying NMR structures (**Supplementary Figure S2**).

Comparing the  $\alpha 9$ -ECD/RgIA complex with the structures of AChBPs in their complexes with other  $\alpha$ -Ctxs, a strikingly high structural similarity was observed for the bound toxins (**Figure 2A**), despite their differences in sequence composition and length (**Figure 2B**). Specifically, upon superposition of the  $\alpha 9$ -ECD bound to RgIA with the protomers of AChBPs bound to other  $\alpha$ -Ctxs, it was revealed that RgIA has an RMSD value for all paired C $\alpha$  atoms of 0.773 Å with PnIA (PDB ID: 2BR8) (Celie et al., 2005), 0.778 Å with PeIA (PDB ID: 5JME) (Hone et al., 2018), 0.702 Å with ImI (PDB ID: 2C9T) (Ulens et al., 2006), 0.865 Å with TxIA (PDB ID: 2UZ6) (Dutertre et al., 2007), 1.013 Å with BuIA (PDB ID: 4EZ1), 1.059 Å with GIC (PDB ID: 5CO5) (Lin et al., 2016) and of 1.321 or 0.979 Å with LsIA

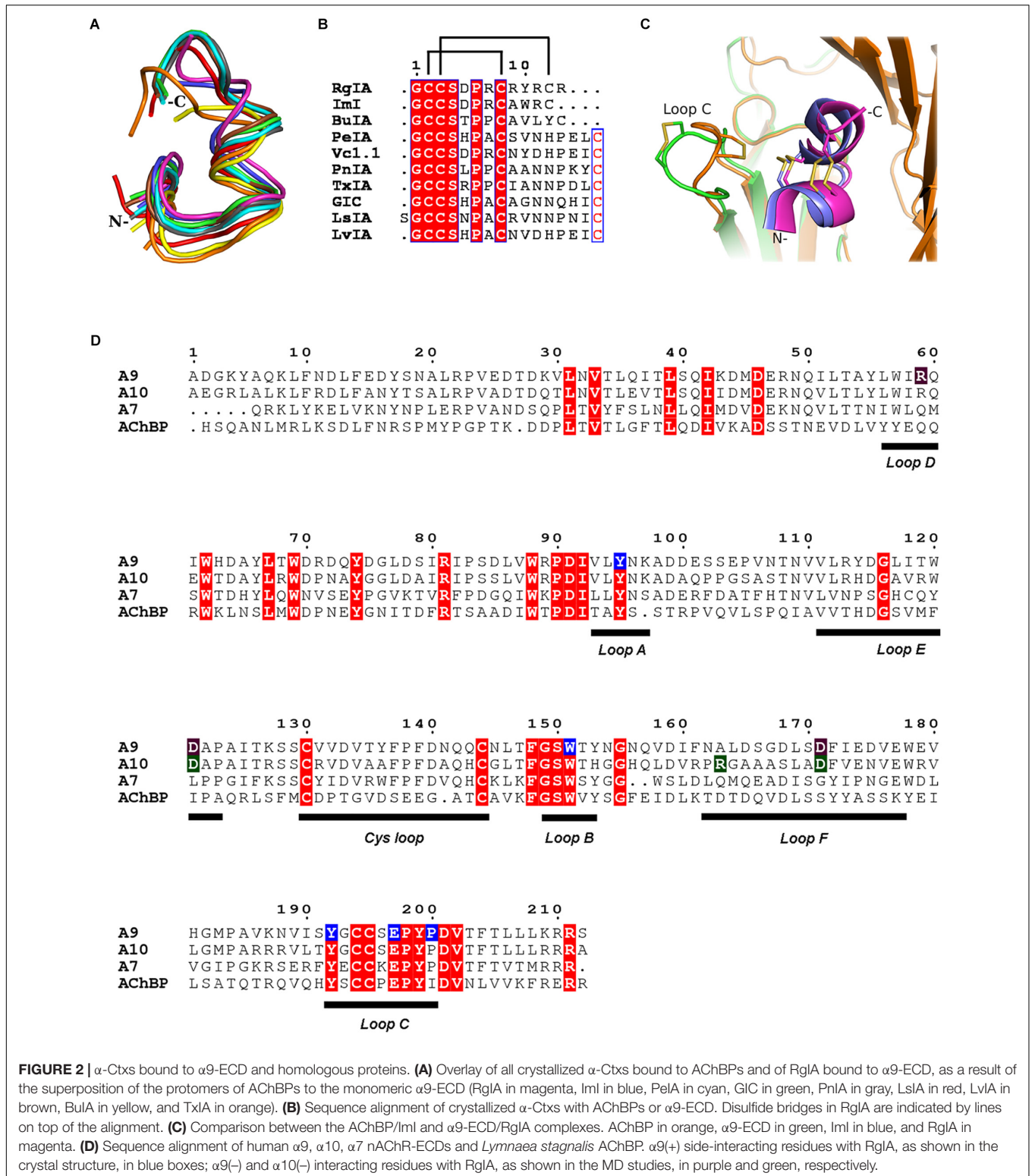


**FIGURE 2** |  $\alpha$ -Ctxs bound to  $\alpha 9$ -ECD and homologous proteins. **(A)** Overlay of all crystallized  $\alpha$ -Ctxs bound to AChBPs and of RgIA bound to  $\alpha 9$ -ECD, as a result of the superposition of the protomers of AChBPs to the monomeric  $\alpha 9$ -ECD (RgIA in magenta, ImI in blue, PeIA in cyan, GIC in green, PnIA in gray, LsIA in red, LvIA in brown, BuIA in yellow, and TxIA in orange). **(B)** Sequence alignment of crystallized  $\alpha$ -Ctxs with AChBPs or  $\alpha 9$ -ECD. Disulfide bridges in RgIA are indicated by lines on top of the alignment. **(C)** Comparison between the AChBP/ImI and  $\alpha 9$ -ECD/RgIA complexes. AChBP in orange,  $\alpha 9$ -ECD in green, ImI in blue, and RgIA in magenta. **(D)** Sequence alignment of human  $\alpha 9$ ,  $\alpha 10$ ,  $\alpha 7$  nAChR-ECDs and *Lymanaea stagnalis* AChBP.  $\alpha 9$ (+) side-interacting residues with RgIA, as shown in the crystal structure, in blue boxes;  $\alpha 9$ (-) and  $\alpha 10$ (-) interacting residues with RgIA, as shown in the MD studies, in purple and green, respectively.

(PDB ID: 5T90) (Abraham et al., 2017) or LvIA (PDB ID: 5XGL) (Xu et al., 2017), respectively.

Thus, all  $\alpha$ -Ctxs in the above complexes adopt similar orientations, but they may be further grouped into three distinct

clusters, regarding their backbone trajectories in the above complexes. The  $\alpha 4/3$ -Ctxs ImI and RgIA comprise the first group, the  $\alpha 4/7$ -Ctxs GIC, LsIA, LvIA, PeIA, and PnIA fall into the second group and the  $\alpha 4/4$ -Ctx BuIA is grouped together with the

$\alpha 4/7$ -Ctx TxIA (Supplementary Figure S3). The members of the first and second groups present an apparent spatial coincidence up to their ninth residue, with RgIA and ImI deviating beyond this point from the other toxins, which on the other hand form a two-turn extended  $\alpha$ -helical domain (Supplementary Figure S3). RgIA and ImI are identical up to their Cys8 residue and differ in two residues at positions 9 and 10 (ImI-Ala9 and ImI-Trp10 vs. RgIA-Arg9 and RgIA-Tyr10) with RgIA being longer than ImI by a C-terminal Arg residue (Figure 2B).

Taken the above into consideration, despite  $\alpha 9$ -ECD being in a monomeric state, it binds  $\alpha$ -Ctx-RgIA in a similar fashion to that of binding of other  $\alpha$ -Ctxs to the pentameric AChBPs (Figure 2A), as previously shown for the complexes of  $\alpha 9$ -ECD with  $\alpha$ -Bgtx and MLA (Zouridakis et al., 2014). This becomes more evident in Figure 2C, which shows the overall very good superposition between the complexes of  $\alpha 9$ -ECD with RgIA and of AChBP with ImI (Ulens et al., 2006). The above observations suggest that the resolved structure presented here depicts accurately the orientation of RgIA in the binding sites of pentameric  $\alpha 9\alpha 10$  nAChRs where  $\alpha 9$  contributes its (+) side. It should be mentioned that the crystal packing contacts between the bound RgIA and an adjacent symmetric  $\alpha 9$ -ECD, contributing to the stabilization of the  $\alpha 9$ -ECD/RgIA complex, affected only the orientation of the side chain of RgIA-Tyr10, as revealed after comparison to its counterpart ImI-Trp10 in the crystal structure of ImI bound to AChBP (Supplementary Figure S4).

## Interactions of RgIA With $\alpha 9$ -ECD

Upon binding, RgIA is buried in the (+) side of  $\alpha 9$ -ECD (Figure 1A) and shares a common orientation with other previously determined  $\alpha$ -Ctxs bound to AChBPs (Figures 2A,C). Its central helical domain protrudes toward the binding site, while its N- and C-termini are located at the bottom and top of the binding site, respectively (Figures 1A, 2C).

The most profound interactions of RgIA with the (+) side of  $\alpha 9$ -ECD involve its aspartic residue at position 5 and its arginine residues at positions 7 and 11 (Figures 1D, 2B). RgIA-Asp5 forms a H-bond with loop-C  $\alpha 9$ -Tyr192, RgIA-Arg7 forms H-bonds with the carbonyl oxygen of loop-C Pro200 and the hydroxyl group of loop-A Tyr95, while RgIA-Arg11 makes a salt bridge with loop-C Glu197 (Figure 1D). Additionally, RgIA-Pro6 makes van der Waals interactions with the loop-B Trp151. Notably, the similar  $\alpha 4/3$ -Ctx ImI makes identical interactions with the (+) side of the binding site of AChBP (Hansen et al., 2005; Ulens et al., 2006), which nevertheless involve highly conserved residues among AChBPs and nAChR  $\alpha$  subunits.

## Radio-Ligand Competition Experiments

The binding affinity of  $\alpha$ -Ctx RgIA to  $\alpha 9$ -ECD was determined via competition experiments, using the monomeric glycosylated or deglycosylated  $\alpha 9$ -ECD and radiolabeled [ $^{125}$ I]- $\alpha$ -Bgtx (Figure 3). The  $K_i$  values for the two  $\alpha 9$ -ECDs, differing in their glycosylation state, were slightly different, with the deglycosylated  $\alpha 9$ -ECD (the one co-crystallized with RgIA) having  $2.7 \pm 0.3 \mu\text{M}$ , and the glycosylated one having  $13.3 \pm 1.5 \mu\text{M}$ . Therefore, one could suggest that the interactions presented in the obtained

crystal structure with the deglycosylated  $\alpha 9$ -ECD, depict those occurring in the case of the glycosylated native  $\alpha 9\alpha 10$  nAChRs, concerning the  $\alpha 9(+)$  side. Also, these  $K_i$  values are in the low micromolar range, as the calculated  $\text{IC}_{50}$  values for RgIA in human  $\alpha 9\alpha 10$  nAChRs (Azam and McIntosh, 2012).

## Molecular Modeling and MD Simulations of Pentameric Human $\alpha 9\alpha 10$ ECDs

With the aim to gain more information about the potential interactions between  $\alpha$ -Ctx RgIA and the ligand-binding sites of human  $\alpha 9\alpha 10$  nAChR, we modeled both possible stoichiometries of the  $\alpha 9\alpha 10$  nAChR ECD (Indurthi et al., 2014), namely  $(\alpha 9)_2(\alpha 10)_3$  and  $(\alpha 9)_3(\alpha 10)_2$  (Figure 4), based on the crystal structures of the complexes  $\alpha 9$ -ECD/RgIA (Figure 1A) and AChBP/ImI (Ulens et al., 2006). In the case of the  $(\alpha 9)_3(\alpha 10)_2$ , an additional binding site is formed between  $\alpha 9$  ECDs (Indurthi et al., 2014), apart from that between  $\alpha 9$  and  $\alpha 10$  ECDs in the  $(\alpha 9)_2(\alpha 10)_3$  stoichiometry (Plazas et al., 2005). One RgIA molecule was modeled in the  $\alpha 9(+)/\alpha 9(-)$  or in the  $\alpha 9(+)/\alpha 10(-)$  binding site in the  $(\alpha 9)_3(\alpha 10)_2$  ECD model (Figures 4A,C), or in the  $\alpha 10(+)/\alpha 9(-)$  binding site in

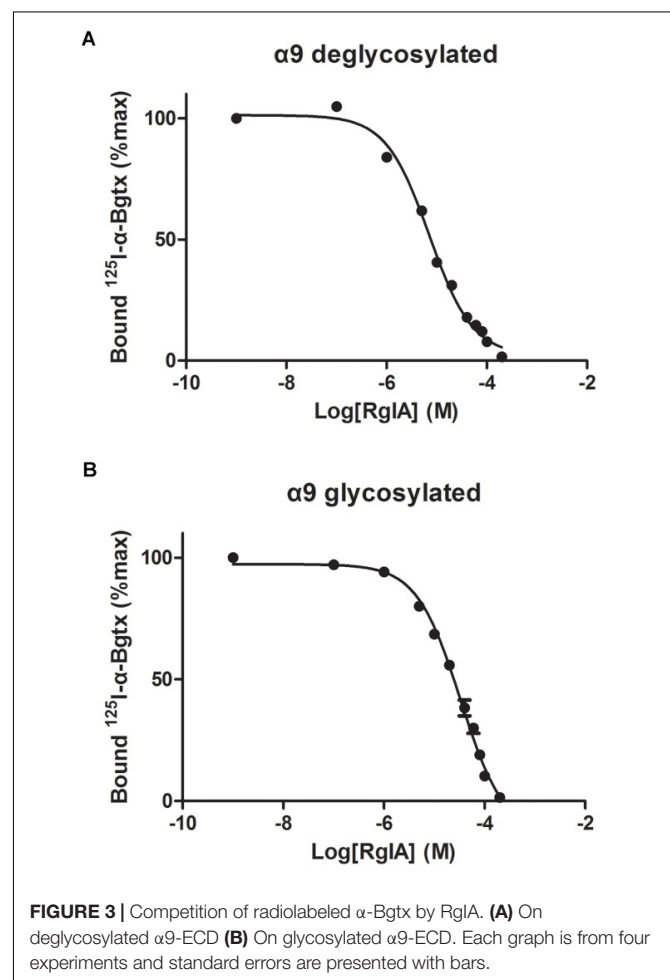
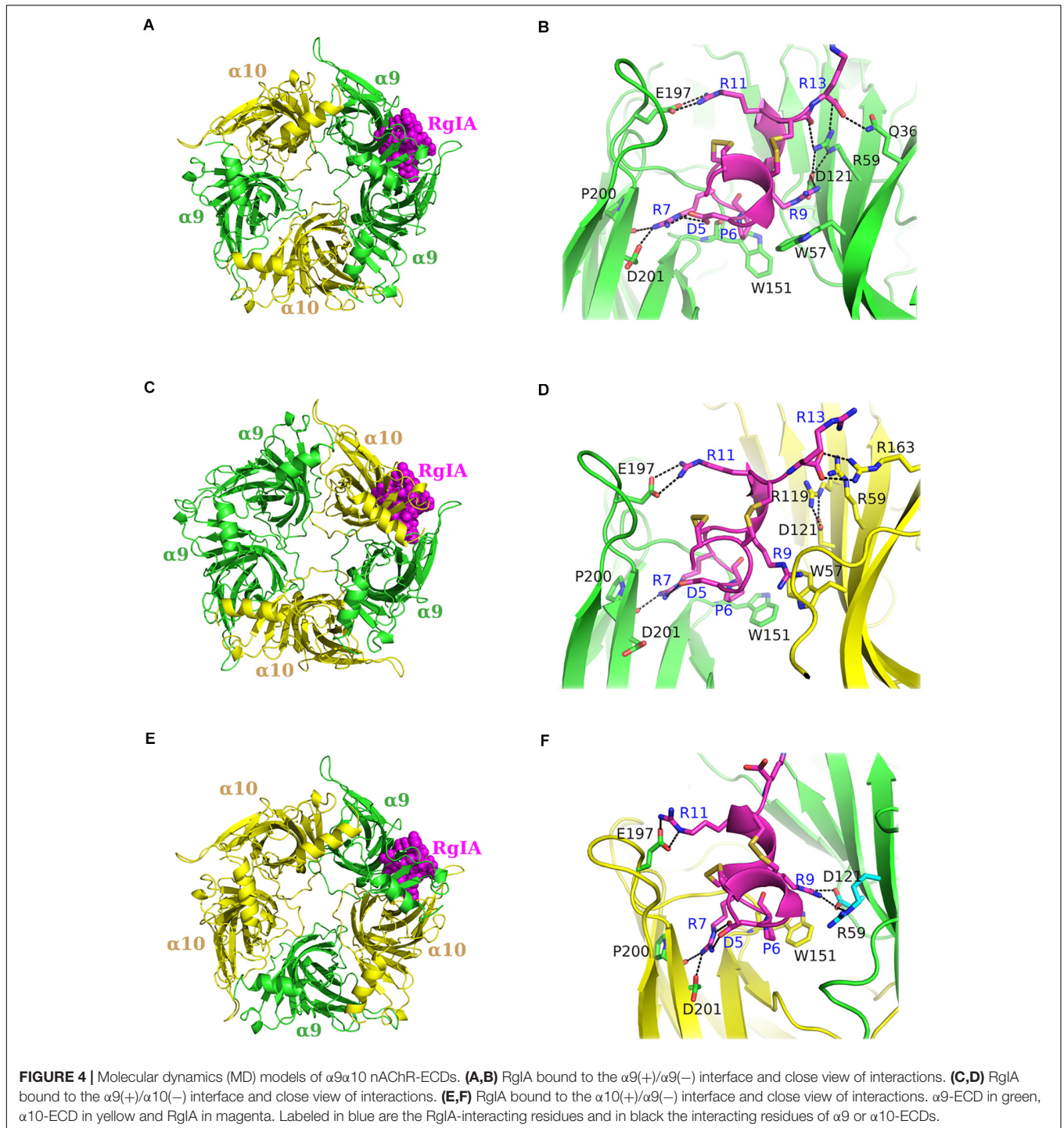


**FIGURE 3** | Competition of radiolabeled  $\alpha$ -Bgtx by RgIA. (A) On deglycosylated  $\alpha 9$ -ECD (B) On glycosylated  $\alpha 9$ -ECD. Each graph is from four experiments and standard errors are presented with bars.



the model of  $(\alpha 9)_2(\alpha 10)_3$  ECD (**Figure 4E**) (all constructed models are provided as **Supplementary Material** in pdb format). Subsequently, we employed MD simulations for the modeled complexes.

Our MDs revealed that the interactions of RgIA at the (+) sides of the binding sites conferred by  $\alpha 9$  or  $\alpha 10$  ECDs were almost identical, given the high sequence similarity (77%) between these ECDs (**Figure 2D**). More

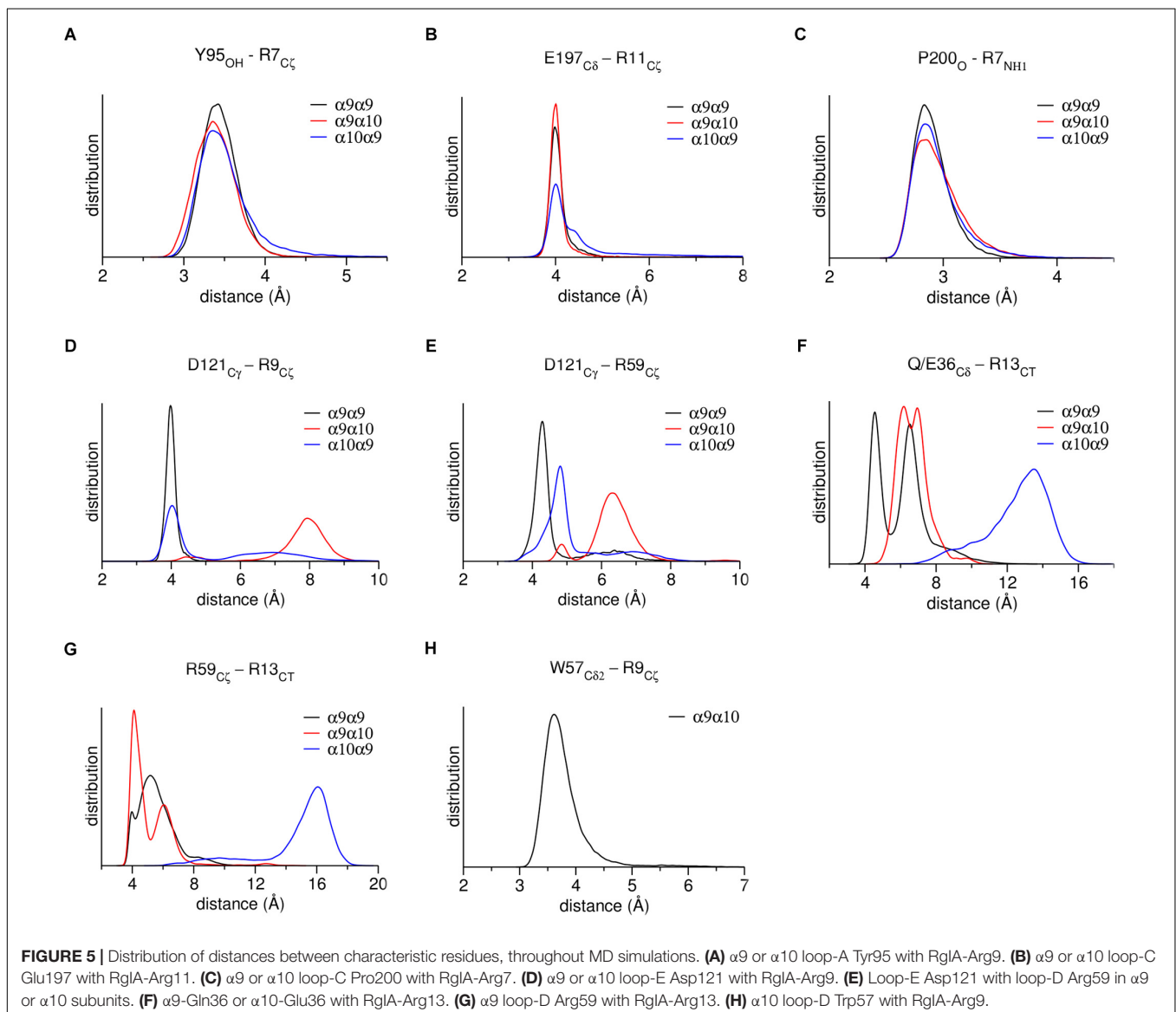
specifically, the conserved residues Tyr95 and Glu197 formed a hydrogen bond and a salt bridge with RgIA Arg7 and Arg11, respectively, while the conserved Pro200 interacted with a strong hydrogen bond with RgIA-Arg7 (**Figures 4B,D,F**). These interactions were retained throughout the MD simulations (**Figures 5A–C**) and were essentially identical to those shown in the crystal structure of  $\alpha 9$ -ECD with RgIA (**Figure 1D**). In addition, similarly to the

crystal structure, RgIA-Pro6 interacts favorably with the loop-B Trp151 of both  $\alpha 9(+)$  and  $\alpha 10(+)$  sides via  $\text{CH}_2\text{-}\pi$  interactions (Figures 4B,D,F).

At the  $\alpha 9(-)$  side of either  $\alpha 9(+)/\alpha 9(-)$  or  $\alpha 10(+)/\alpha 9(-)$  binding sites (Figures 4A,E), Asp121 and RgIA-Arg9 formed a salt bridge (Figures 4B,F), which was stable throughout the course of MD simulations (Figure 5D). At both binding sites,  $\alpha 9$ -Asp121 formed a stable intramolecular interaction with  $\alpha 9$ -Arg59 (Figures 4B,F, 5E), an interaction present in all previous  $\alpha 9$ -ECD crystal structures (Zouridakis et al., 2014), as well as in the  $\alpha 9$ -ECD/RgIA structure, presented here. In the  $\alpha 9(+)/\alpha 9(-)$  binding site, distinctly to the  $\alpha 10(+)/\alpha 9(-)$  binding site, the MD simulations revealed interactions between  $\alpha 9$ -Gln36 and  $\alpha 9$ -Arg59 with the carboxylate group of the RgIA C-terminus (Figure 4B), which however were short-lived (Figures 5F,G), probably due to

the high mobility of the RgIA C-terminus, and thus should be considered only transient.

At the  $\alpha 10(-)$  side of the  $\alpha 9(+)/\alpha 10(-)$  binding site (Figures 4C,D), a complete different motif of interactions with RgIA was revealed, probably due to the high accumulation of arginine residues at the  $\alpha 10(-)$  side (Figure 4D). Interestingly,  $\alpha 10$ -ECD bears two additional arginine residues at positions 119 and 163 of its  $(-)$  side compared to  $\alpha 9$ -ECD (Figures 2D, 4D). The stable interaction observed between Asp121 and RgIA-Arg9, when  $\alpha 9$  is involved in the  $(-)$  side, is no longer present, nor is the intramolecular bond between Asp121 and Arg59 (Figures 4D, 5D,E). Instead, other intramolecular interactions, such as those between Asp121 and Arg119 or between Arg59 and Glu61, stabilize the  $\alpha 10(-)$  side, but its interactions with RgIA are rather aberrant and transient, apart from the cation- $\pi$  interaction between  $\alpha 10$ -Trp57 and RgIA-Arg9 (Figures 4D, 5H).



## DISCUSSION

In this study, we determined the crystal structure of the complex of human neuronal nAChR  $\alpha 9$ -ECD with  $\alpha$ -Ctx RgIA, revealing the interactions of RgIA with the  $\alpha 9(+)$  side (**Figures 1A,D**). The interaction motif of RgIA with  $\alpha 9$ -ECD is identical to that of  $\alpha$ -Ctx ImI with AChBP (Hansen et al., 2005; Ulens et al., 2006), since the involved residues of the two  $\alpha$ -Ctxs are identical and the interacting residues of both proteins are highly conserved. Both  $\alpha$ -Ctxs interact with  $\alpha 9(+)$  or AChBP(+) sides through their Asp-Pro-Arg triad of loop 1 and a conserved Arg at position 11 (**Figure 2B**). These observations comply with previous mutational studies, which had shown the critical role of the Asp-Pro-Arg triad to the inhibitory potency of RgIA on  $\alpha 9\alpha 10$  nAChRs (Ellison et al., 2006, 2008).

Moreover, since the complex of the monomeric  $\alpha 9$ -ECD with RgIA superimposed very well with the complexes of the pentameric AChBPs with ImI (**Figure 2C**) and other  $\alpha$ -Ctxs (**Figure 2A**), this study showed that the (+) side of the  $\alpha 9$ -ECD alone is adequate to determine the orientation of the bound RgIA. This is similar to previous observations for the complexes of the monomeric  $\alpha 9$ -ECD with the antagonists MLA and  $\alpha$ -Bgtx (Zouridakis et al., 2014). The  $K_i$  value of RgIA binding to the deglycosylated  $\alpha 9$ -ECD was calculated to be 2.7  $\mu$ M, similar to that for the glycosylated protein (13  $\mu$ M), which is the form more close to the native  $\alpha 9$  subunit (**Figure 3**). Taking also into account that the  $IC_{50}$  value of RgIA to human  $\alpha 9\alpha 10$  nAChRs is also at the low micromolar range ( $\sim 0.5$   $\mu$ M) (Azam and McIntosh, 2012), the interactions revealed in the structure of the deglycosylated  $\alpha 9$ -ECD with RgIA are very likely to depict the ones occurring in the  $\alpha 9(+)$  side-containing binding sites of native human  $\alpha 9\alpha 10$  nAChRs.

Notably,  $\alpha 9$  and  $\alpha 10$  ECDs have a remarkable sequence similarity of 77%, which is even higher for the regions participating in the (+) side (loops A, B, and C) of the binding site (**Figure 2D**). In particular, the (+) sides of the two ECDs differ only in one residue at position 153;  $\alpha 10$  has a histidine residue in contrast to tyrosine in  $\alpha 9$  and all other nAChR  $\alpha$ -subunits. However, this highly conserved tyrosine, as shown in the crystal structures of  $\alpha 9$ -ECD and other homologous proteins (e.g., Brejc et al., 2001; Kouvatzos et al., 2016; Morales-Perez et al., 2016), faces toward the interior of the protein and has not been considered a binding determinant in nAChRs (Hansen et al., 2005; Ulens et al., 2006). Thus, since the  $\alpha 9(+)$  and  $\alpha 10(+)$  sides are almost identical, one can expect that the  $\alpha 10(+)$  side could also bind RgIA similarly.

Given that  $\alpha 9\alpha 10$  nAChRs may contain three putative binding sites, namely the  $\alpha 9(+)/\alpha 9(-)$ ,  $\alpha 9(+)/\alpha 10(-)$ , and the  $\alpha 10(+)/\alpha 9(-)$  (Plazas et al., 2005; Ellison et al., 2008; Azam and McIntosh, 2012; Indurthi et al., 2014; Azam et al., 2015; Boffi et al., 2017), we performed MD simulations in order to assess possible preference of RgIA for any of these sites, conferred by the non-conserved (-) sides of  $\alpha 9$  or  $\alpha 10$  ECDs. Previous attempts of modeling the complex of RgIA with the ECD of  $\alpha 9\alpha 10$  nAChR have yielded controversial results: Perez et al. (2009) suggested that the favorable binding site for RgIA is the  $\alpha 9(+)/\alpha 10(-)$ , whereas Azam et al. (2015)

proposed the  $\alpha 10(+)/\alpha 9(-)$ , complying with their mutational and electrophysiological data. However, these models were based on the X-ray crystal structures of either the AChBP/ImI complex alone (Ulens et al., 2006), or on the  $\alpha 9$ -ECD apo structure (Zouridakis et al., 2014) and AChBP/ImI complex. In the current study, the X-ray structure of  $\alpha 9$ -ECD in complex with RgIA was used as a template together with the AChBP/ImI complex for modeling of the binding sites of the human  $\alpha 9\alpha 10$  nAChR.

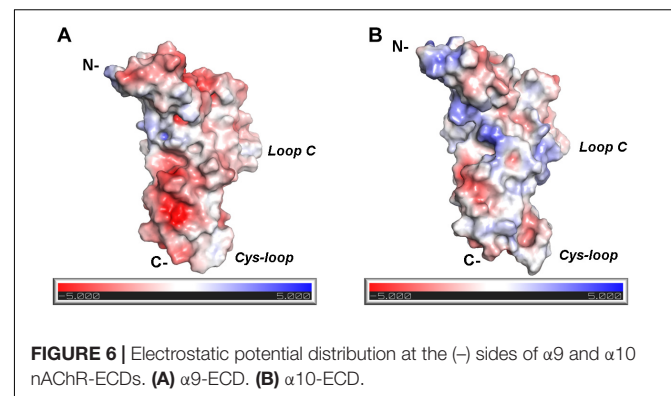
As expected, due to the substantial similarity of the (+) sides of  $\alpha 9$  and  $\alpha 10$  ECDs, the MD studies showed that RgIA forms similar interactions with them (**Figures 4B,D,F**), some of which have been previously evaluated by mutational studies. The mutation  $\alpha 9$ -Trp151 to threonine has led to a  $\sim 10$ -fold increase of the  $IC_{50}$  value of RgIA to  $\alpha 9\alpha 10$  nAChRs (Ellison et al., 2008), while the single-point mutations Glu197Gln or Pro200Gln at the  $\alpha 10(+)$  side have shown a  $\sim 20$ - or  $\sim 400$ -fold decrease in the potency of RgIA to  $\alpha 9\alpha 10$  nAChRs (Azam et al., 2015).

Instead, the interactions formed between RgIA and the non-conserved (-) sides of  $\alpha 9$  or  $\alpha 10$  ECDs are significantly different:

(a) At the  $\alpha 9(+)/\alpha 9(-)$  and  $\alpha 10(+)/\alpha 9(-)$  interfaces, the (-) side of  $\alpha 9$ -ECD forms a critical salt bridge between  $\alpha 9$ -Asp121 and RgIA-Arg9 (**Figures 4B,F, 5D**). This interaction was previously shown to be very important for the potency of both ACh and RgIA on  $\alpha 9\alpha 10$  nAChRs, since mutation  $\alpha 9$ -Asp121Leu increased the corresponding  $EC_{50}$  or  $IC_{50}$  values by  $\sim 30$  times or by three orders of magnitude, respectively (Azam et al., 2015).

(b) At the  $\alpha 9(+)/\alpha 10(-)$  interface, where the (-) side of  $\alpha 10$ -ECD is densely populated by positively charged residues (**Figures 4D, 6**), the interaction of Asp121 with RgIA-Arg9, shown at the  $\alpha 9(+)/\alpha 9(-)$  and  $\alpha 10(+)/\alpha 9(-)$  interfaces, is disrupted; instead,  $\alpha 10$ -Asp121 makes an intramolecular salt bridge with  $\alpha 10$ -Arg119, whereas RgIA-Arg9 makes a cation- $\pi$  interaction with the  $\alpha 10$ -Trp57 (**Figure 4D**). However, this interaction in  $\alpha 9(+)/\alpha 10(-)$  interfaces, if applicable in nature, could not justify the selectivity of RgIA on  $\alpha 9\alpha 10$  nAChRs, since this loop-D tryptophan residue is invariant among all nAChR subunits. The observations for the modeled  $\alpha 9(+)/\alpha 10(-)$  interface comply with previous functional data which showed that the mutation  $\alpha 10$ -Asp121Leu did not affect the inhibitory potency of RgIA on  $\alpha 9\alpha 10$  nAChRs (Azam et al., 2015).

The differences in the binding motif of RgIA with the  $\alpha 10(-)$  side compared to the  $\alpha 9(-)$  side may be attributed to repulsive



forces between the profoundly more positively charged  $\alpha 10(-)$  side (**Figure 6**) and the positively charged RgIA. A first indication supporting the role of electrostatics in the binding of RgIA is the calculated non-bonded interaction energies extracted from the MD simulations of each pentameric assembly. The electrostatic term of the interaction energy ( $E_{elec}$ ) was calculated to be  $-743 \pm 37$  kcal/mol for  $\alpha 9(+)\alpha 9(-)$ ,  $-620 \pm 87$  kcal/mol for  $\alpha 10(+)\alpha 9(-)$ , and  $-498 \pm 86$  kcal/mol for  $\alpha 9(-)\alpha 10(+)$ . The corresponding van der Waals interaction energy terms ( $E_{vdW}$ ) are calculated to be  $-95 \pm 11$  kcal/mol  $\alpha 9(+)\alpha 9(-)$ ,  $-74 \pm 10$  kcal/mol for  $\alpha 10(+)\alpha 9(-)$ , and  $-69 \pm 17$  kcal/mol for  $\alpha 9(+)\alpha 10(-)$ . In addition, the interface areas formed by two adjacent subunits with bound RgIA, in the cases of  $\alpha 9(+)/\alpha 9(-)$  and  $\alpha 10(+)/\alpha 9(-)$  are  $1084 \pm 121 \text{ \AA}^2$  and  $1050 \pm 80 \text{ \AA}^2$ , respectively, close to the experimentally determined one ( $1194 \pm 33 \text{ \AA}^2$ ) from the structure of AChBP with  $\alpha$ -Ctx Iml (Ulens et al., 2006). Instead, in the case of  $\alpha 9(+)/\alpha 10(-)$ , the interface area is significantly lower ( $685 \pm 79 \text{ \AA}^2$ ), indicating a rather aberrant assembly between these two subunits in the presence of  $\alpha$ -Ctx RgIA. Taken together, our results indicate the lower affinity of RgIA binding at the  $\alpha 9(+)\alpha 10(-)$  site with respect to the  $\alpha 9(+)\alpha 9(-)$  and  $\alpha 10(+)\alpha 9(-)$ , in well agreement with previous mutational and functional data, which have shown that the (+) side of RgIA binding is conferred by either  $\alpha 9$  or  $\alpha 10$  subunits (Ellison et al., 2008; Azam et al., 2015) and the (-) side by  $\alpha 9$  rather than  $\alpha 10$  (Azam and McIntosh, 2012; Azam et al., 2015). It seems plausible that the arginine residues at positions 119 and 163 at the (-) side of  $\alpha 10$ -ECD, which in the case of  $\alpha 9$  correspond to threonine and alanine, respectively (**Figure 2D**), contribute critically to the repulsion of  $\alpha$ -Ctx RgIA in  $\alpha 10(-)$  side-containing binding sites. It is noteworthy that  $\alpha 10$  is the only nAChR  $\alpha$ -subunit bearing charged residues at these sites.

In the presented crystal structure of the complex of  $\alpha 9$ -ECD with RgIA, and in the structures of the free  $\alpha 9$ -ECD and of its complexes with  $\alpha$ -Bgtx and MLA (Zouridakis et al., 2014), Asp121 forms a stable salt bridge with the adjacent Arg59. Notably, these charged residues are uniquely present in the  $\alpha 9$  and  $\alpha 10$  nAChR subunits. Our MD simulations showed that this interaction was retained in the  $\alpha 9(-)$  side in both  $\alpha 9(+)/\alpha 9(-)$  and  $\alpha 10(+)/\alpha 9(-)$  binding sites, but was disrupted in the  $\alpha 10(-)$  side throughout the simulations (**Figure 5E**), despite its presence in the initial  $\alpha 10$ -ECD model. Thus, in the case of the  $\alpha 9(+)/\alpha 10(-)$  binding site, where the (-) side of  $\alpha 10$ -ECD is more positively charged, structural rearrangements of residues at the  $\alpha 10(-)$  side occurred in the course of MD simulations, in order to accommodate the also positively charged RgIA, leading to different interactions with RgIA (**Figure 4D**) compared to those with the  $\alpha 9(-)$  side (**Figures 4B,F**).

Interestingly, other  $\alpha 9\alpha 10$  selective  $\alpha$ -Ctxs are PeIA and Vc1.1, which despite being  $\alpha 4/7$ -Ctxs, have a potency for the rat  $\alpha 9\alpha 10$  nAChR ( $IC_{50}$  of 7 or 19 nM, respectively) comparable with that of RgIA ( $IC_{50} = 4.5$  nM) (McIntosh et al., 2005; Clark et al., 2006; Vincler et al., 2006). PeIA and Vc1.1 have almost identical loop-2 compositions, but completely different than that of RgIA (**Figure 2B**). In addition, PeIA lacks the loop-1 Asp-Pro-Arg triad, shown to make critical interactions with the  $\alpha 9(+)$  side

in the  $\alpha 9$ -ECD/RgIA crystal structure and with the (+) sides of the presented  $\alpha 9\alpha 10$  nAChR-ECD models. Thus, the selectivity of these  $\alpha$ -Ctxs to  $\alpha 9\alpha 10$  nAChRs has to deal with other interactions than those between RgIA and the receptor.

Several models of pain and inflammation have demonstrated that  $\alpha 9\alpha 10$  nAChRs play a role in modulating the pathophysiology associated with neuropathic pain (Di Cesare Mannelli et al., 2014; Pacini et al., 2016). The analgesic and anti-inflammatory effects of RgIA and Vc1.1 via inhibition of the  $\alpha 9\alpha 10$  nAChR have also been demonstrated (Satkunanathan et al., 2005; Vincler et al., 2006). However, it has been proposed that the effects of these  $\alpha$ -Ctxs can also be transmitted via inhibition of GABA $\beta$  receptors (Callaghan et al., 2008; Sadeghi et al., 2017). Vc1.1 was tested as the first nAChR-targeting  $\alpha$ -Ctx for the treatment of neuropathic pain, but since it was demonstrated that, similarly to RgIA (Azam and McIntosh, 2012), Vc1.1 was several orders of magnitude less potent in humans than in rats (Terlau and Olivera, 2004; Halai et al., 2009), clinical trials were discontinued. The difference in potency of RgIA between human and rat  $\alpha 9\alpha 10$  nAChRs has been attributed to a specific residue located at position 61 of  $\alpha 9$  (Ile in humans vs. Thr in rats), at its (-) side (Azam and McIntosh, 2012). Previous MD studies indicated that this threonine residue in rat  $\alpha 9\alpha 10$  nAChRs coordinates a network of interactions within  $\alpha 9$  (-) side, facilitating the binding of RgIA to these receptors (Azam et al., 2015). Efforts to improve the potency of RgIA in human  $\alpha 9\alpha 10$  nAChRs have led to an over 1000-fold more potent analog (RgIA4) (Romero et al., 2017), shown to be an effective analgesic in a model of neuropathic pain (Christensen et al., 2017; Romero et al., 2017), while being highly selective for  $\alpha 9\alpha 10$  nAChRs over GABA $\beta$  receptors. Notably, in this analog, among other drastic changes, the positively charged Arg residues at positions 9, 11, and 13 were replaced by the neutral citrulline, Qln, and Tyr residues, respectively. These replacements have probably alleviated the repulsive forces between RgIA and (-) sides of  $\alpha 9\alpha 10$  nAChRs, while maintaining the ability of RgIA to make interactions with  $\alpha 9\alpha 10$  nAChRs, but via H-bonding. However, in order to deeply understand the interactions of RgIA4 with  $\alpha 9\alpha 10$  nAChRs, additional detailed structural studies involving RgIA4 are needed. The findings of the present study, showing the actual interactions of RgIA with the (+) side of the human  $\alpha 9$ -ECD and the indicative interactions in the fully assembled binding sites of the human  $\alpha 9\alpha 10$  nAChR ECD, may be helpful for the design of improved therapeutic analogs.

## CONCLUSION

The first crystal structure of a human nAChR domain with an  $\alpha$ -Ctx is presented. The structure revealed the interactions between  $\alpha$ -Ctx RgIA and the (+) side of neuronal nAChR  $\alpha 9$ -ECD in high detail. Based on the structure of this complex, models of human  $\alpha 9\alpha 10$  nAChR ECD with fully formed binding sites were constructed with RgIA bound to each of them. Our MD simulations suggest that the favorable binding site of RgIA in the human  $\alpha 9\alpha 10$  nAChR ECD consists of either  $\alpha 9$  or

$\alpha 10$  subunits as the (+) side and of an adjacent  $\alpha 9$  rather than  $\alpha 10$  subunit as the (–) side. The results of this study may be helpful to medicinal chemists for design of improved RgIA analogs targeting the human  $\alpha 9\alpha 10$  nAChR against auditory diseases and neuropathic pain.

## AUTHOR CONTRIBUTIONS

MZ and PG conceived the project, expressed and purified  $\alpha 9$ -ECD, conducted the competition experiments, crystallized the complex of  $\alpha 9$ -ECD with  $\alpha$ -Ctx RgIA and solved the crystal structure. PG, MZ, and IK designed the experiments. II and IK synthesized and purified the  $\alpha$ -Ctx RgIA and AP performed and analyzed the MD simulations. PG, MZ, and AP wrote the manuscript. ST and VT contributed to management of the project

## REFERENCES

- Abraham, N., Healy, M., Ragnarsson, L., Brust, A., Alewood, P. F., and Lewis, R. J. (2017). Structural mechanisms for alpha-conotoxin activity at the human alpha3beta4 nicotinic acetylcholine receptor. *Sci. Rep.* 7:45466. doi: 10.1038/srep45466
- Afonine, P. V., Grosse-Kunstleve, R. W., Echols, N., Headd, J. J., Moriarty, N. W., Mustyakimov, M., et al. (2012). Towards automated crystallographic structure refinement with phenix.refine. *Acta Crystallogr. D Biol. Crystallogr.* 68(Pt 4), 352–367. doi: 10.1107/S0907444912001308
- Albuquerque, E. X., Pereira, E. F., Alkondon, M., and Rogers, S. W. (2009). Mammalian nicotinic acetylcholine receptors: from structure to function. *Physiol. Rev.* 89, 73–120. doi: 10.1152/physrev.00015.2008
- Azam, L., and McIntosh, J. M. (2009). Alpha-conotoxins as pharmacological probes of nicotinic acetylcholine receptors. *Acta Pharmacol. Sin.* 30, 771–783. doi: 10.1038/aps.2009.47
- Azam, L., and McIntosh, J. M. (2012). Molecular basis for the differential sensitivity of rat and human alpha9alpha10 nAChRs to alpha-conotoxin RgIA. *J. Neurochem.* 122, 1137–1144. doi: 10.1111/j.1471-4159.2012.07867.x
- Azam, L., Papakyriakou, A., Zouridakis, M., Giastas, P., Tzartos, S. J., and McIntosh, J. M. (2015). Molecular interaction of alpha-conotoxin RgIA with the rat alpha9alpha10 nicotinic acetylcholine receptor. *Mol. Pharmacol.* 87, 855–864. doi: 10.1124/mol.114.096511
- Beckmann, J., and Lips, K. S. (2013). The non-neuronal cholinergic system in health and disease. *Pharmacology* 92, 286–302. doi: 10.1159/000355835
- Boffi, J. C., Marcovich, I., Gill-Thind, J. K., Corradi, J., Collins, T., Lipovsek, M. M., et al. (2017). Differential contribution of subunit interfaces to alpha9alpha10 nicotinic acetylcholine receptor function. *Mol. Pharmacol.* 91, 250–262. doi: 10.1124/mol.116.107482
- Bourne, Y., Sulzenbacher, G., Radic, Z., Araoz, R., Reynaud, M., Benoit, E., et al. (2015). Marine macrocyclic imines, pinnatoxins A and G: structural determinants and functional properties to distinguish neuronal alpha7 from muscle alpha1(2)betagammadelta nAChRs. *Structure* 23, 1106–1115. doi: 10.1016/j.str.2015.04.009
- Brejč, K., van Dijk, W. J., Klaassen, R. V., Schuurmans, M., van Der Oost, J., Smit, A. B., et al. (2001). Crystal structure of an ACh-binding protein reveals the ligand-binding domain of nicotinic receptors. *Nature* 411, 269–276. doi: 10.1038/35077011
- Callaghan, B., Haythornthwaite, A., Berecki, G., Clark, R. J., Craik, D. J., and Adams, D. J. (2008). Analgesic alpha-conotoxins Vc1.1 and RgIA inhibit N-type calcium channels in rat sensory neurons via GABAB receptor activation. *J. Neurosci.* 28, 10943–10951. doi: 10.1523/JNEUROSCI.3594-08.2008
- Case, D. A., Cheatham, T. E. III, Darden, T., Gohlke, H., Luo, R., Merz, K. M., et al. (2005). The Amber biomolecular simulation programs. *J. Comput. Chem.* 26, 1668–1688. doi: 10.1002/jcc.20290
- Celie, P. H., Kasheverov, I. E., Mordvintsev, D. Y., Hogg, R. C., van Nierop, P., van Elk, R., et al. (2005). Crystal structure of nicotinic acetylcholine receptor homolog AChBP in complex with an alpha-conotoxin PnIA variant. *Nat. Struct. Mol. Biol.* 12, 582–588. doi: 10.1038/nsmb951
- Celie, P. H., van Rossum-Fikkert, S. E., van Dijk, W. J., Brejč, K., Smit, A. B., and Sixma, T. K. (2004). Nicotine and carbamylcholine binding to nicotinic acetylcholine receptors as studied in AChBP crystal structures. *Neuron* 41, 907–914. doi: 10.1016/s0896-6273(04)00115-1
- Chi, S. W., Kim, D. H., Olivera, B. M., McIntosh, J. M., and Han, K. H. (2004). Solution conformation of alpha-conotoxin GIC, a novel potent antagonist of alpha3beta2 nicotinic acetylcholine receptors. *Biochem. J.* 380(Pt 2), 347–352. doi: 10.1042/BJ20031792
- Chi, S. W., Kim, D. H., Olivera, B. M., McIntosh, J. M., and Han, K. H. (2006). NMR structure determination of alpha-conotoxin BuIA, a novel neuronal nicotinic acetylcholine receptor antagonist with an unusual 4/4 disulfide scaffold. *Biochem. Biophys. Res. Commun.* 349, 1228–1234. doi: 10.1016/j.bbrc.2006.08.164
- Christensen, S. B., Hone, A. J., Roux, I., Kniazeff, J., Pin, J. P., Upert, G., et al. (2017). RgIA4 potently blocks mouse alpha9alpha10 nAChRs and provides long lasting protection against oxaliplatin-induced cold allodynia. *Front. Cell. Neurosci.* 11:219. doi: 10.3389/fncel.2017.00219
- Clark, R. J., Daly, N. L., Halai, R., Nevin, S. T., Adams, D. J., and Craik, D. J. (2008). The three-dimensional structure of the analgesic alpha-conotoxin, RgIA. *FEBS Lett.* 582, 597–602. doi: 10.1016/j.febslet.2008.01.027
- Clark, R. J., Fischer, H., Nevin, S. T., Adams, D. J., and Craik, D. J. (2006). The synthesis, structural characterization, and receptor specificity of the alpha-conotoxin Vc1.1. *J. Biol. Chem.* 281, 23254–23263. doi: 10.1074/jbc.M604550200
- Dellisanti, C. D., Yao, Y., Stroud, J. C., Wang, Z. Z., and Chen, L. (2007). Crystal structure of the extracellular domain of nAChR alpha1 bound to alpha-bungarotoxin at 1.94 Å resolution. *Nat. Neurosci.* 10, 953–962. doi: 10.1038/nn1942
- Di Cesare Mannelli, L., Cinci, L., Micheli, L., Zanardelli, M., Pacini, A., McIntosh, J. M., et al. (2014). alpha-conotoxin RgIA protects against the development of nerve injury-induced chronic pain and prevents both neuronal and glial derangement. *Pain* 155, 1986–1995. doi: 10.1016/j.pain.2014.06.023
- Dineley, K. T., Pandya, A. A., and Yakel, J. L. (2015). Nicotinic ACh receptors as therapeutic targets in CNS disorders. *Trends Pharmacol. Sci.* 36, 96–108. doi: 10.1016/j.tips.2014.12.002

and edited the manuscript. All authors reviewed and approved the manuscript.

## FUNDING

This work was supported by a grant from Stavros Niarchos Foundation (ST and MZ), by RSF (Grant No. 16-14-00215) (VT and II), by RFBR (Grant No. 18-04-01366) (IK), by the Hellenic Foundation for Research and Innovation (HFRI) and the General Secretariat for Research and Technology (PG), (StruNic, Grant No. 677) and by BioStruct-X (Contract No. 283570/3521).

## SUPPLEMENTARY MATERIAL

The Supplementary Material for this article can be found online at: <https://www.frontiersin.org/articles/10.3389/fphar.2019.00474/full#supplementary-material>

- Dutertre, S., Ulens, C., Buttner, R., Fish, A., van Elk, R., Kendel, Y., et al. (2007). AChBP-targeted alpha-conotoxin correlates distinct binding orientations with nAChR subtype selectivity. *EMBO J.* 26, 3858–3867. doi: 10.1038/sj.emboj.7601785
- Elgoyhen, A. B., Johnson, D. S., Boulter, J., Vetter, D. E., and Heinemann, S. (1994). Alpha 9: an acetylcholine receptor with novel pharmacological properties expressed in rat cochlear hair cells. *Cell* 79, 705–715. doi: 10.1016/0092-8674(94)90555-X
- Elgoyhen, A. B., Katz, E., and Fuchs, P. A. (2009). The nicotinic receptor of cochlear hair cells: a possible pharmacotherapeutic target? *Biochem. Pharmacol.* 78, 712–719. doi: 10.1016/j.bcp.2009.05.023
- Elgoyhen, A. B., and Langguth, B. (2010). Pharmacological approaches to the treatment of tinnitus. *Drug Discov. Today* 15, 300–305. doi: 10.1016/j.drudis.2009.11.003
- Elgoyhen, A. B., Vetter, D. E., Katz, E., Rothlin, C. V., Heinemann, S. F., and Boulter, J. (2001). alpha10: a determinant of nicotinic cholinergic receptor function in mammalian vestibular and cochlear mechanosensory hair cells. *Proc. Natl. Acad. Sci. U.S.A.* 98, 3501–3506. doi: 10.1073/pnas.051622798
- Ellison, M., Feng, Z. P., Park, A. J., Zhang, X., Olivera, B. M., McIntosh, J. M., et al. (2008). Alpha-RgIA, a novel conotoxin that blocks the alpha9alpha10 nAChR: structure and identification of key receptor-binding residues. *J. Mol. Biol.* 377, 1216–1227. doi: 10.1016/j.jmb.2008.01.082
- Ellison, M., Haberlandt, C., Gomez-Casati, M. E., Watkins, M., Elgoyhen, A. B., McIntosh, J. M., et al. (2006). Alpha-RgIA: a novel conotoxin that specifically and potently blocks the alpha9alpha10 nAChR. *Biochemistry* 45, 1511–1517. doi: 10.1021/bi0520129
- Emsley, P., Lohkamp, B., Scott, W. G., and Cowtan, K. (2010). Features and development of coot. *Acta Crystallogr. D Biol. Crystallogr.* 66(Pt 4), 486–501. doi: 10.1107/S0907444910007493
- Engel, A. G., Shen, X. M., Selcen, D., and Sine, S. M. (2015). Congenital myasthenic syndromes: pathogenesis, diagnosis, and treatment. *Lancet Neurol.* 14, 420–434. doi: 10.1016/s1474-4422(14)70201-7
- Evans, P. (2006). Scaling and assessment of data quality. *Acta Crystallogr. D Biol. Crystallogr.* 62(Pt 1), 72–82. doi: 10.1107/S0907444905036693
- Evans, P. R. (2011). An introduction to data reduction: space-group determination, scaling and intensity statistics. *Acta Crystallogr. D Biol. Crystallogr.* 67(Pt 4), 282–292. doi: 10.1107/S090744491003982X
- Fiser, A., and Sali, A. (2003). Modeller: generation and refinement of homology-based protein structure models. *Methods Enzymol.* 374, 461–491. doi: 10.1016/S0076-6879(03)74020-8
- Gehrmann, J., Daly, N. L., Alewood, P. F., and Craik, D. J. (1999). Solution structure of alpha-conotoxin ImI by 1H nuclear magnetic resonance. *J. Med. Chem.* 42, 2364–2372. doi: 10.1021/jm990114p
- Giastas, P., Zouridakis, M., and Tzartos, S. J. (2018). Understanding structure-function relationships of the human neuronal acetylcholine receptor: insights from the first crystal structures of neuronal subunits. *Br. J. Pharmacol.* 175, 1880–1891. doi: 10.1111/bph.13838
- Gotti, C., Moretti, M., Gaimarri, A., Zanardi, A., Clementi, F., and Zoli, M. (2007). Heterogeneity and complexity of native brain nicotinic receptors. *Biochem. Pharmacol.* 74, 1102–1111. doi: 10.1016/j.bcp.2007.05.023
- Gotti, C., Zoli, M., and Clementi, F. (2006). Brain nicotinic acetylcholine receptors: native subtypes and their relevance. *Trends Pharmacol. Sci.* 27, 482–491. doi: 10.1016/j.tips.2006.07.004
- Halai, R., Clark, R. J., Nevin, S. T., Jensen, J. E., Adams, D. J., and Craik, D. J. (2009). Scanning mutagenesis of alpha-conotoxin Vc1.1 reveals residues crucial for activity at the alpha9alpha10 nicotinic acetylcholine receptor. *J. Biol. Chem.* 284, 20275–20284. doi: 10.1074/jbc.M109.015339
- Hansen, S. B., Sulzenbacher, G., Huxford, T., Marchot, P., Taylor, P., and Bourne, Y. (2005). Structures of Aplysia AChBP complexes with nicotinic agonists and antagonists reveal distinctive binding interfaces and conformations. *EMBO J.* 24, 3635–3646. doi: 10.1038/sj.emboj.7600828
- Hecker, A., Kullmar, M., Wilker, S., Richter, K., Zakrzewicz, A., Atanasova, S., et al. (2015). Phosphocholine-modified macromolecules and canonical nicotinic agonists inhibit ATP-induced IL-1beta release. *J. Immunol.* 195, 2325–2334. doi: 10.4049/jimmunol.1400974
- Hone, A. J., and McIntosh, J. M. (2018). Nicotinic acetylcholine receptors in neuropathic and inflammatory pain. *FEBS Lett.* 592, 1045–1062. doi: 10.1002/1873-3468.12884
- Hone, A. J., Talley, T. T., Bobango, J., Huidobro Melo, C., Hararah, F., Gajewiak, J. B., et al. (2018). Molecular determinants of alpha-conotoxin potency for inhibition of human and rat alpha6beta4 nicotinic acetylcholine receptors. *J. Biol. Chem.* 293, 17838–17852. doi: 10.1074/jbc.RA118.005649
- Hopkins, C. W., Le Grand, S., Walker, R. C., and Roitberg, A. E. (2015). Long-time-step molecular dynamics through hydrogen mass repartitioning. *J. Chem. Theory Comput.* 11, 1864–1874. doi: 10.1021/ct5010406
- Hu, S. H., Gehrmann, J., Guddat, L. W., Alewood, P. F., Craik, D. J., and Martin, J. L. (1996). The 1.1 A crystal structure of the neuronal acetylcholine receptor antagonist, alpha-conotoxin PnIA from *Conus pennaceus*. *Structure* 4, 417–423. doi: 10.1016/s0969-2126(96)00047-0
- Humphrey, W., Dalke, A., and Schulten, K. (1996). VMD: visual molecular dynamics. *J. Mol. Graph.* 14, 33–38, 27–28.
- Indurthi, D. C., Pera, E., Kim, H. L., Chu, C., McLeod, M. D., McIntosh, J. M., et al. (2014). Presence of multiple binding sites on alpha9alpha10 nAChR receptors alludes to stoichiometric-dependent action of the alpha-conotoxin, Vc1.1. *Biochem. Pharmacol.* 89, 131–140. doi: 10.1016/j.bcp.2014.02.002
- Janes, R. W. (2005). alpha-Conotoxins as selective probes for nicotinic acetylcholine receptor subclasses. *Curr. Opin. Pharmacol.* 5, 280–292. doi: 10.1016/j.coph.2005.01.013
- Kabsch, W. (2010). Xds. *Acta Crystallogr. D Biol. Crystallogr.* 66(Pt 2), 125–132. doi: 10.1107/S0907444909047337
- Karplus, P. A., and Diederichs, K. (2012). Linking crystallographic model and data quality. *Science* 336, 1030–1033. doi: 10.1126/science.1218231
- Kouvatsos, N., Giastas, P., Chroni-Tzartou, D., Pouloupoulou, C., and Tzartos, S. J. (2016). Crystal structure of a human neuronal nAChR extracellular domain in pentameric assembly: ligand-bound alpha2 homopentamer. *Proc. Natl. Acad. Sci. U.S.A.* 113, 9635–9640. doi: 10.1073/pnas.1602619113
- Lester, H. A., Dibas, M. I., Dahan, D. S., Leite, J. F., and Dougherty, D. A. (2004). Cys-loop receptors: new twists and turns. *Trends Neurosci.* 27, 329–336. doi: 10.1016/j.tins.2004.04.002
- Li, S. X., Huang, S., Bren, N., Noridomi, K., Dellisanti, C. D., Sine, S. M., et al. (2011). Ligand-binding domain of an alpha7-nicotinic receptor chimera and its complex with agonist. *Nat. Neurosci.* 14, 1253–1259. doi: 10.1038/nn.2908
- Lin, B., Xu, M., Zhu, X., Wu, Y., Liu, X., Zhangsun, D., et al. (2016). From crystal structure of alpha-conotoxin GIC in complex with Ac-AChBP to molecular determinants of its high selectivity for alpha3beta2 nAChR. *Sci. Rep.* 6:22349. doi: 10.1038/srep22349
- Luo, S., Zhangsun, D., Schroeder, C. I., Zhu, X., Hu, Y., Wu, Y., et al. (2014). A novel alpha4/7-conotoxin LvIA from *Conus lividus* that selectively blocks alpha3beta2 vs. alpha6/alpha3beta2beta3 nicotinic acetylcholine receptors. *FASEB J.* 28, 1842–1853. doi: 10.1096/fj.13-244103
- Lustig, L. R., Peng, H., Hiel, H., Yamamoto, T., and Fuchs, P. A. (2001). Molecular cloning and mapping of the human nicotinic acetylcholine receptor alpha10 (CHRNA10). *Genomics* 73, 272–283. doi: 10.1006/geno.2000.6503
- Maier, J. A., Martinez, C., Kasavajhala, K., Wickstrom, L., Hauser, K. E., and Simmerling, C. (2015). ff14SB: improving the accuracy of protein side chain and backbone parameters from ff99SB. *J. Chem. Theory Comput.* 11, 3696–3713. doi: 10.1021/acs.jctc.5b00255
- Maslennikov, I. V., Shenkarev, Z. O., Zhmak, M. N., Ivanov, V. T., Methfessel, C., Tsetlin, V. I., et al. (1999). NMR spatial structure of alpha-conotoxin ImI reveals a common scaffold in snail and snake toxins recognizing neuronal nicotinic acetylcholine receptors. *FEBS Lett.* 444, 275–280. doi: 10.1016/s0014-5793(99)00069-1
- McCoy, A. J., Grosse-Kunstleve, R. W., Adams, P. D., Winn, M. D., Storoni, L. C., and Read, R. J. (2007). Phaser crystallographic software. *J. Appl. Crystallogr.* 40(Pt 4), 658–674. doi: 10.1107/S0021889807021206
- McIntosh, J. M., Plazas, P. V., Watkins, M., Gomez-Casati, M. E., Olivera, B. M., and Elgoyhen, A. B. (2005). A novel alpha-conotoxin, PeIA, cloned from *Conus pergrandis*, discriminates between rat alpha9alpha10 and alpha7 nicotinic cholinergic receptors. *J. Biol. Chem.* 280, 30107–30112. doi: 10.1074/jbc.M504102200
- Millar, N. S., and Gotti, C. (2009). Diversity of vertebrate nicotinic acetylcholine receptors. *Neuropharmacology* 56, 237–246. doi: 10.1016/j.neuropharm.2008.07.041
- Morales-Perez, C. L., Noviello, C. M., and Hibbs, R. E. (2016). X-ray structure of the human alpha4beta2 nicotinic receptor. *Nature* 538, 411–415. doi: 10.1038/nature19785

- Nemecz, A., Prevost, M. S., Menny, A., and Corringer, P. J. (2016). Emerging molecular mechanisms of signal transduction in pentameric ligand-gated ion channels. *Neuron* 90, 452–470. doi: 10.1016/j.neuron.2016.03.032
- Nemecz, A., and Taylor, P. (2011). Creating an  $\alpha 7$  nicotinic acetylcholine recognition domain from the acetylcholine-binding protein: crystallographic and ligand selectivity analyses. *J. Biol. Chem.* 286, 42555–42565. doi: 10.1074/jbc.M111.286583
- Nicke, A., Wonnacott, S., and Lewis, R. J. (2004). Alpha-conotoxins as tools for the elucidation of structure and function of neuronal nicotinic acetylcholine receptor subtypes. *Eur. J. Biochem.* 271, 2305–2319. doi: 10.1111/j.1432-1033.2004.04145.x
- Pacini, A., Micheli, L., Maresca, M., Branca, J. J., McIntosh, J. M., Ghelardini, C., et al. (2016). The  $\alpha 9\alpha 10$  nicotinic receptor antagonist alpha-conotoxin RgIA prevents neuropathic pain induced by oxaliplatin treatment. *Exp. Neurol.* 282, 37–48. doi: 10.1016/j.expneurol.2016.04.022
- Peng, H., Ferris, R. L., Matthews, T., Hiel, H., Lopez-Albaitero, A., and Lustig, L. R. (2004). Characterization of the human nicotinic acetylcholine receptor subunit alpha ( $\alpha$ ) 9 (CHRNA9) and alpha ( $\alpha$ ) 10 (CHRNA10) in lymphocytes. *Life Sci.* 76, 263–280. doi: 10.1016/j.lfs.2004.05.031
- Perez, E. G., Cassels, B. K., and Zapata-Torres, G. (2009). Molecular modeling of the  $\alpha 9\alpha 10$  nicotinic acetylcholine receptor subtype. *Bioorg. Med. Chem. Lett.* 19, 251–254. doi: 10.1016/j.bmcl.2008.10.094
- Plazas, P. V., Katz, E., Gomez-Casati, M. E., Bouzat, C., and Elgoyhen, A. B. (2005). Stoichiometry of the  $\alpha 9\alpha 10$  nicotinic cholinergic receptor. *J. Neurosci.* 25, 10905–10912. doi: 10.1523/JNEUROSCI.3805-05.2005
- Quik, M., Bordia, T., Huang, L., and Perez, X. (2011). Targeting nicotinic receptors for Parkinson's disease therapy. *CNS Neurol. Disord. Drug Targets* 10, 651–658. doi: 10.2174/187152711797247849
- Romero, H. K., Christensen, S. B., Di Cesare Mannelli, L., Gajewiak, J., Ramachandra, R., Elmslie, K. S., et al. (2017). Inhibition of  $\alpha 9\alpha 10$  nicotinic acetylcholine receptors prevents chemotherapy-induced neuropathic pain. *Proc. Natl. Acad. Sci. U.S.A.* 114, E1825–E1832. doi: 10.1073/pnas.1621433114
- Rucktooa, P., Smit, A. B., and Sixma, T. K. (2009). Insight in nAChR subtype selectivity from AChBP crystal structures. *Biochem. Pharmacol.* 78, 777–787. doi: 10.1016/j.bcp.2009.06.098
- Sadeghi, M., McArthur, J. R., Finol-Urdaneta, R. K., and Adams, D. J. (2017). Analgesic conopeptides targeting G protein-coupled receptors reduce excitability of sensory neurons. *Neuropharmacology* 127, 116–123. doi: 10.1016/j.neuropharm.2017.05.020
- Salomon-Ferrer, R., Gotz, A. W., Poole, D., Le Grand, S., and Walker, R. C. (2013). Routine microsecond molecular dynamics simulations with AMBER on GPUs. 2. Explicit solvent particle mesh Ewald. *J. Chem. Theory Comput.* 9, 3878–3888. doi: 10.1021/ct400314y
- Satkunathan, N., Livett, B., Gayler, K., Sandall, D., Down, J., and Khalil, Z. (2005). Alpha-conotoxin Vc1.1 alleviates neuropathic pain and accelerates functional recovery of injured neurones. *Brain Res.* 1059, 149–158. doi: 10.1016/j.brainres.2005.08.009
- Shahsavari, A., Ahring, P. K., Olsen, J. A., Krintel, C., Kastrop, J. S., Balle, T., et al. (2015). Acetylcholine-binding protein engineered to mimic the  $\alpha 4\text{-}\alpha 4$  binding pocket in  $\alpha 4\beta 2$  nicotinic acetylcholine receptors reveals interface specific interactions important for binding and activity. *Mol. Pharmacol.* 88, 697–707. doi: 10.1124/mol.115.098061
- Sine, S. M., and Engel, A. G. (2006). Recent advances in Cys-loop receptor structure and function. *Nature* 440, 448–455. doi: 10.1038/nature04708
- Taly, A., Corringer, P. J., Guedin, D., Lestage, P., and Changeux, J. P. (2009). Nicotinic receptors: allosteric transitions and therapeutic targets in the nervous system. *Nat. Rev. Drug Discov.* 8, 733–750. doi: 10.1038/nrd2927
- Terlau, H., and Olivera, B. M. (2004). Conus venoms: a rich source of novel ion channel-targeted peptides. *Physiol. Rev.* 84, 41–68. doi: 10.1152/physrev.00020.2003
- Tsetlin, V., Utkin, Y., and Kasheverov, I. (2009). Polypeptide and peptide toxins, magnifying lenses for binding sites in nicotinic acetylcholine receptors. *Biochem. Pharmacol.* 78, 720–731. doi: 10.1016/j.bcp.2009.05.032
- Ukens, C., Hogg, R. C., Celie, P. H., Bertrand, D., Tsetlin, V., Smit, A. B., et al. (2006). Structural determinants of selective  $\alpha$ -conotoxin binding to a nicotinic acetylcholine receptor homolog AChBP. *Proc. Natl. Acad. Sci. U.S.A.* 103, 3615–3620. doi: 10.1073/pnas.0507889103
- Unwin, N. (1995). Acetylcholine receptor channel imaged in the open state. *Nature* 373, 37–43. doi: 10.1038/373037a0
- Unwin, N. (2005). Refined structure of the nicotinic acetylcholine receptor at 4 Å resolution. *J. Mol. Biol.* 346, 967–989. doi: 10.1016/j.jmb.2004.12.031
- Vinclair, M., Wittenauer, S., Parker, R., Ellison, M., Olivera, B. M., and McIntosh, J. M. (2006). Molecular mechanism for analgesia involving specific antagonism of  $\alpha 9\alpha 10$  nicotinic acetylcholine receptors. *Proc. Natl. Acad. Sci. U.S.A.* 103, 17880–17884. doi: 10.1073/pnas.0608715103
- Walsh, R. M. Jr., Roh, S. H., Gharpure, A., Morales-Perez, C. L., Teng, J., and Hibbs, R. E. (2018). Structural principles of distinct assemblies of the human  $\alpha 4\beta 2$  nicotinic receptor. *Nature* 557, 261–265. doi: 10.1038/s41586-018-0081-7
- Wessler, I., and Kirkpatrick, C. J. (2008). Acetylcholine beyond neurons: the non-neuronal cholinergic system in humans. *Br. J. Pharmacol.* 154, 1558–1571. doi: 10.1038/bjp.2008.185
- Winn, M. D., Ballard, C. C., Cowtan, K. D., Dodson, E. J., Emsley, P., Evans, P. R., et al. (2011). Overview of the CCP4 suite and current developments. *Acta Crystallogr. D Biol. Crystallogr.* 67(Pt 4), 235–242. doi: 10.1107/S0907444910045749
- Xu, M., Zhu, X., Yu, J., Luo, S., and Wang, X. (2017). The crystal structure of Ac-AChBP in complex with  $\alpha$ -conotoxin Lv1A reveals the mechanism of its selectivity towards different nAChR subtypes. *Protein Cell* 8, 675–685. doi: 10.1007/s13238-017-0426-2
- Zouridakis, M., Giastas, P., Zarkadas, E., Chroni-Tzartou, D., Bregestovski, P., and Tzartos, S. J. (2014). Crystal structures of free and antagonist-bound states of human  $\alpha 9$  nicotinic receptor extracellular domain. *Nat. Struct. Mol. Biol.* 21, 976–980. doi: 10.1038/nsmb.2900

**Conflict of Interest Statement:** The authors declare that the research was conducted in the absence of any commercial or financial relationships that could be construed as a potential conflict of interest.

Copyright © 2019 Zouridakis, Papakyriakou, Ivanov, Kasheverov, Tsetlin, Tzartos and Giastas. This is an open-access article distributed under the terms of the Creative Commons Attribution License (CC BY). The use, distribution or reproduction in other forums is permitted, provided the original author(s) and the copyright owner(s) are credited and that the original publication in this journal is cited, in accordance with accepted academic practice. No use, distribution or reproduction is permitted which does not comply with these terms.